JACS
JOURNAL OF THE AMERICAN CHEMICAL SOCIETY
Communication
pubs.acs.org/JACS

Microporous Aluminophosphate Nanosheets and Their Nanomorphic Zeolite Analogues Tailored by Hierarchical Structure-Directing Amines

Yongbeom Seo,[†,‡] Sungjune Lee,[†,‡] Changbum Jo,[†,‡] and Ryong Ryoo*[,†,‡]

[†]Center for Nanomaterials and Chemical Reactions, Institute for Basic Science (IBS), Daejeon 305-701, Republic of Korea
[‡]Department of Chemistry, KAIST, Daejeon 305-701, Republic of Korea

Supporting Information

ABSTRACT: Multiamines with amphiphilic structures have been synthesized to serve as simultaneous structure-directing agents in micro- and meso-structural levels for aluminophosphate materials (AlPOs) and their analogues, such as silicoaluminophosphate, cobalt aluminophosphate, and gallium phosphate. The amine molecules are assembled into a micelle with a specific morphology to function as a meso-level structure director. Individual amine groups in the micelle are able to direct the formation of microporous crystalline AlPO structure. The resultant meso-level morphologies of the AlPOs are typically nanosheets of uniform thickness, which can be tailored in the range of 2−5 nm by the number of amine groups. Sponge-like disordered mesoporous morphologies can be generated, depending on the amine structures. Using such multiamines provides a versatile route to various phosphate materials with a structural hierarchy for enhanced porous functionalities.

Inorganic phosphates with a nanostructure attract considerable attention because of their widespread applications.[1−9] For example, synthetic hydroxyapatite ($CaPO_4$) can be clinically used for artificial bone implantation.[4,5] Silicoaluminophosphates (SAPOs) can be used as microporous solid acid catalysts and as other catalytic materials that support metal nanoparticles.[3,6,7] Recently, lithium iron phosphate ($LiFePO_4$) has been spotlighted as a cathode material in lithium-ion batteries.[8,9] Various phosphate materials can be synthesized with nanoporous structures, and as nanoparticles, and other nanomorphic forms by cooperative assemblage between an inorganic phosphate and an organic structure-directing agent (SDA).[10−14] The organic SDA molecules can function as a template or guide for inorganic crystal growth into a specific nanomorphology. Synthesis of porous hydroxyapatite nanocrystals in the presence of poly(acrylic acid) or polyglutamates is one of the examples.[10,11] Crystalline microporous aluminophosphates (AlPOs) and their structural analogues, such as SAPOs, can be synthesized using organic amines as the microporous SDA.[12−14] Due to the regular arrangement of micropores with extremely narrow pore size distribution, AlPO families of various pore diameters have been used in gas separation, adsorption, and host−guest chemistry.[3,14,15] One of the great merits of AlPOs is that various transition metals (Ti, Cr, Mn, Fe, Co, etc.) in addition to Si can be incorporated in the porous framework by substitution of Al or P.[3,16] As a result of metal incorporation, the physicochemical properties of the AlPOs can be changed remarkably. If Si atoms are introduced, the AlPO framework possesses Brönsted and Lewis acid sites that can catalyze various reactions, such as methanol-to-olefin transformation, hydroisomerization, and esterification.[6,7,17,18] Transition-metal-containing AlPOs can be used as catalysts for various redox reactions.[3,19] Microporous crystalline AlPOs are normally obtained as micrometer-sized crystals. Such AlPO crystals are thousands of times larger than the framework pores (typically, <1 nm in diameter) and are called bulk crystals. Often, bulk AlPO crystals suffer from diffusion limitations, similar to their well-known structural analogue, zeolite.[20]

Herein, we report that AlPOs and their structural analogues could be synthesized with nanosheet morphologies of only 2 nm thickness, using multiamines with amphiphilic structure like a surfactant as an SDA. The porous structures and morphologies of the AlPOs were characterized using powder XRD, SEM, TEM, solid-state ^{27}Al and ^{31}P MAS NMR, and N_2 adsorption−desorption isotherms. Many of the amine molecules assembled into a micelle with a specific morphology that could function as a meso-level SDA, while individual amine groups functioned as a microporous SDA for the AlPO framework formation. Among the synthesized porous materials, a mesoporous SAPO with crystalline microporous walls (∼5 nm thick) exhibited high catalytic selectivity and longevity for *n*-heptane isomerization compared to bulk SAPO. We show that the hierarchical structure-directing (HSD) AlPO synthesis strategy can be extended to other nanomorphic AlPOs, transition-metal-substituted AlPOs, and even gallium phosphates (GaPOs).

Bulk AlPOs are commonly synthesized via the hydrothermal reaction of phosphoric acid with a suitable aluminum compound (aluminum isopropoxide, aluminum hydroxide, pseudoboehmite, etc.) in the presence of microporous structure-directing, small-molecular amine SDA. Compared to conventional bulk AlPO synthesis, the syntheses of present AlPO nanosheets were performed using the HSD multiamines and multiammoniums shown in Table 1. In brief, the HSD agents (HSDA), pseudoboehmite, and phosphoric acid were well mixed with an aqueous solution (see Supporting

Received: April 10, 2013
Published: June 3, 2013

   dx.doi.org/10.1021/ja403580j | *J. Am. Chem. Soc.* 2013, 135, 8806−8809

Table 1. Structure of HSDAs and Derivative AlPO Products

HSDA structure	HSDA notation	AlPO framework type	morphology thickness
$C_{22}H_{45}-N(CH_3)-C_6H_{12}-N(CH_3)_2$	N^3N^3	AEL	2 nm sheet
$C_{22}H_{45}-NH-C_6H_{12}-NH_2$	N^2N^1	AFI	2 nm sheet
$C_{22}H_{45}-N^+(CH_3)_2-C_6H_{12}-N(CH_3)_2(OH^-)$	N^4N^3	nonporous crystal	1 nm sheet
$C_{22}H_{45}-N^+(CH_3)_2-C_6H_{12}-N^+(CH_3)_2-[CH_2-(C_6H_4)-CH_2-N^+(CH_3)_2-C_6H_{12}-N^+(CH_3)_2]_x-C_{22}H_{45}(OH^-)_{2+2x}$	$4N^4$ for $x = 1$	ATO	3 nm sheet
	$6N^4$ for $x = 2$	ATO	4 nm sheet
	$8N^4$ for $x = 3$	ATO	5 nm sponge

Information (SI) for details). The molar composition of the resultant gel was 1.0 Al_2O_3:1.0 P_2O_5:500 H_2O:x HSDA, where x was varied from 0.125 to 0.5 according to the number of N atoms in HSDA. The pH of the gel mixture was ~3. The mixture was heated in an oven at 453 K with tumbling. The AlPO product was filtered after heating for 24 h. After drying at 373 K, the product was calcined under air flow at 823 K to remove the SDA.

As shown in Table 1, the HSDAs are denoted according to the number of N atoms and degree of the amine. For example, $C_{22}H_{45}-NH-C_6H_{12}-NH_2$ SDA has two N atoms: one for the secondary amine and another for the primary amine. This SDA is therefore denoted N^2N^1, where the superscript '2' indicates 'secondary'. When this compound was used as an SDA, the resultant AlPO product exhibited the XRD pattern denoted 'nano' in Figure 1B. Based on this wide-angle XRD pattern, the small-angle XRD in Figure 1A, and the TEM image in Figure 1D, the structure of this AlPO could be assigned to AEL (10-membered oxygen ring, 1D straight channel). The AlPO had nanosheet morphology with a 2 nm thickness. The nanosheets were arranged in a multilamellar form (Figure 1C,D). In good agreement with the multilamellar type mesostructural organization, the small-angle XRD pattern exhibited three Bragg diffractions at 2θ = 1.40° (d = 6.3 nm), 2.80° (d = 3.15 nm), and 4.20° (d = 2.1 nm). This result indicates that the AEL-type AlPO nanosheets had 2 nm thickness along the crystal c-axis and that the 1D channels were aligned perpendicularly to the nanosheet plane. Because of the extremely thin framework thickness along the c-axis, nanomorphic AlPO showed very weak Bragg reflections for the direction of the c-axis, compared to bulk AEL AlPO. After removing the organic SDA completely through high-temperature calcination, the porous textual properties of the calcined AEL AlPO were evaluated from the N_2 adsorption–desorption isotherms measured at 77 K. The specific surface area was determined by the Brunauer–Emmett–Teller (BET) method. The BET surface area was much higher (296 $m^2\ g^{-1}$) than that of its bulk counterpart (150 $m^2\ g^{-1}$). In agreement with the high BET area, high-resolution TEM and SEM images of the AlPO sample showed that a significant number of nanosheets were still separated to retain mesopores between them (Figure S1). The separation of the nanosheets can be attributed to the mismatching of crystal orientations along the b–c plane and also partial crystal intergrowths that can act as pillars between the nanosheets, similar to the MFI zeolite nanosheets synthesized by multi-ammonium surfactants.[21−24]

The structure of the AlPO nanosheets (as synthesized without calcination) was further investigated with MAS ^{27}Al and ^{31}P NMR spectroscopy. The ^{27}Al NMR spectrum exhibited an intense peak with a chemical shift of 38.0 ppm, a weak signal at 10.3 ppm, and another weak signal at −10.1 ppm (Figure S2A). The main signal at 38.0 ppm was assigned to the tetrahedral Al in the crystalline AlPO framework. The two low-intensity signals could be attributed to hydration of some tetrahedral Al sites into penta- and octa-coordination. As for the ^{27}Al NMR investigation, the nanosheets exhibited no significant differences from bulk AlPO. On the other hand, the ^{31}P NMR spectra showed a significant difference from the spectra of the bulk AlPO, due to the presence of P–OH groups at the external surface. In the bulk AEL AlPO, only a signal at −29 ppm was notable, corresponding to the framework P atoms that had tetrahedral coordination inside crystal. That is, P atoms existing on the external surface were negligible. In the case of the nanosheets, however, there were a large number of P atoms on external surfaces. These P atoms gave an additional intense ^{31}P NMR peak at −19 ppm, and they were assigned to $P(-OAl-)_3(-OH)_1$ (Figure S2B). The presence of the P-bonded hydroxyl groups was analogous to crystal termination with silanol groups, i.e., Si–OH, in zeolite nanosheets.[25] Therefore the present surface P–OH groups may be called 'phosphinol' groups. The chemistry of the phosphinol groups, such as mild acidity,[26] metal coordination and organic functionalization,[27] may be an intriguing subject for the development of new porous catalytic materials in the future.

The HSDAs in Table 1 with different molecular structures yielded various AlPO framework types and mesostructures. The N^2N^1 SDA gave a 2 nm-thick nanosheet of the AFI-type

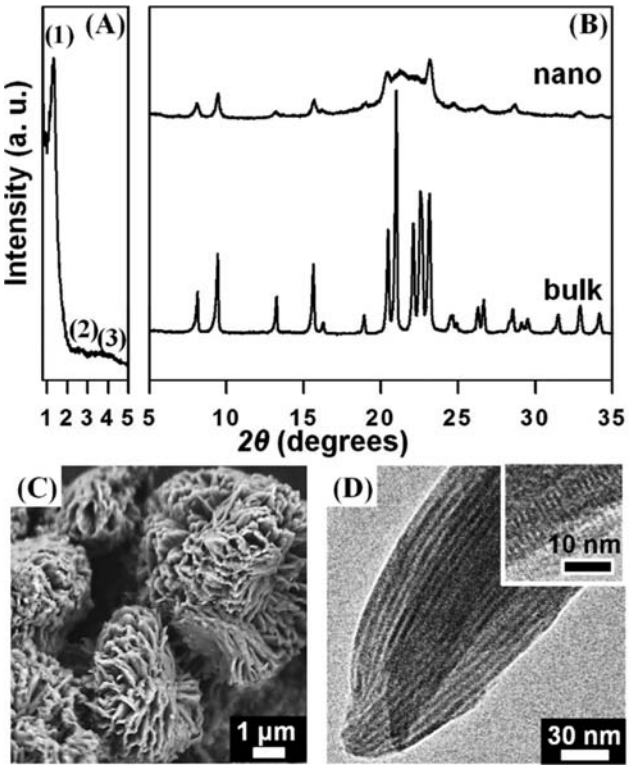

Figure 1. Powder XRD patterns (A,B), SEM (C) and TEM (D) images of AlPO nanosheets constructed with AEL-type microporous crystalline frameworks, as synthesized using $C_{22}H_{45}-N(CH_3)-C_6H_{12}-N(CH_3)_2$. The XRD pattern of bulk AEL AlPO is shown for comparison. Note that short AlPO microporous channels are perpendicular to the wide plane of the nanosheet.

dx.doi.org/10.1021/ja403580j | J. Am. Chem. Soc. 2013, 135, 8806–8809

framework (0.73 nm micropores with 1D channels along the *c*-axis). The nanosheets were layered in a multilamellar mesostructure (Figure S3). On the other hand, N^4N^3 produced a nonporous crystalline AlPO with multilamellar nanosheet morphology. All the gemini-type HSDAs in Table 1 ($4N^4$, $6N^4$, and $8N^4$) generated the same ATO-type AlPO framework (0.54 nm micropore with 1D channels along the *c*-axis), irrespective of the number of N atoms (the wide-angle XRD patterns Figure S4). However, the framework thickness and mesostructure were changed according to the detailed structures of the SDAs (Figures 2 and S4). Notably, the $8N^4$ SDA was able

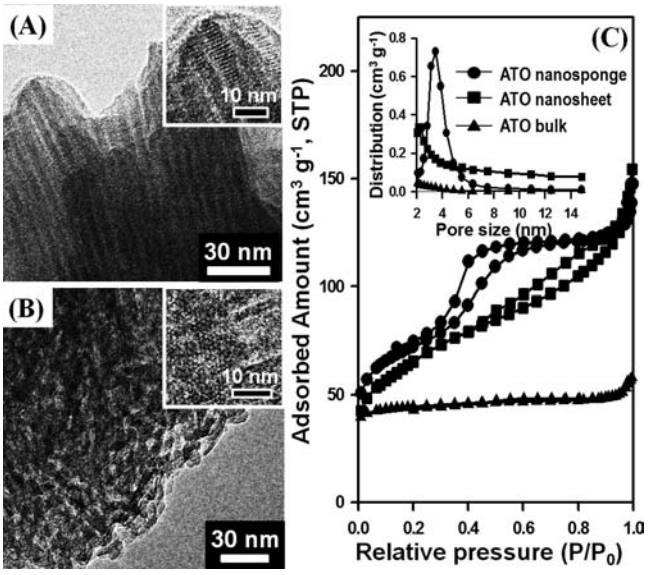

Figure 2. TEM images of microporous crystalline AlPO nanosheets with ATO-type framework structure synthesized using $4N^4$ (A), and nanosponges of the same structure type synthesized using $8N^4$ (B). The pore size distribution curves (C) of these AlPO samples were from N_2 adsorption−desorption isotherms. Note a narrow distribution of mesopore diameters in the AlPO nanosponge, despite disordered mesopores.

to generate a nanosponge-like mesoporous AlPO. Because the ATO nanosponge had 3D intersupporting nanowalls, mesopores could be retained by the nanowalls even after calcination (Figure S5), which was in contrast to the coalescence of nanosheets in the case of N^3N^3 SDA. It was possible to determine the mesopore diameters using N_2 adsorption isotherm. The results showed a very sharp pore size distribution centered at 3.4 nm, which was comparable to pore diameters in an ordered mesoporous silica MCM-41 (Figure 2C). Another notable point is that the mesopore walls of the AlPO material were a crystalline microporous AlPO. The crystalline walls were ~5 nm in thickness, which was determined by TEM image and also by subtracting the mesopore diameter (3.4 nm) from the *d*-spacing (8.1 nm) calculated from the low-angle peak in XRD pattern. The ATO-type AlPO nanosponge exhibited a very high specific BET surface area (335 $m^2\ g^{-1}$), compared to its bulk counterpart (100 $m^2\ g^{-1}$).

It was possible to synthesize a nanomorphic SAPO sample by adding fumed silica as a Si source into the synthesis composition for the aforementioned ATO-type AlPO nanosponge. The SAPO nanosponge had the molar composition of $(Al_{0.58}P_{0.38}Si_{0.05})O_2$, which was analyzed by the inductive coupled plasma spectroscopy after calcinations. The ATO-type SAPO nanosponge exhibited very similar framework acidity to bulk crystal samples, judging from the temperature programmed desorption of NH_3 (Figure S6 and Table S1). The SAPO nanosponge was tested as a catalyst for hydroisomerization of *n*-heptane (i.e., *n*-C_7) after supporting Pt nanoparticles corresponding to 0.5 wt %, using the ion-exchange method.[28] The Pt/SAPO nanosponge was investigated by comparing with a bulk SAPO sample with similar Pt content and metal dispersion (Table S1 and Figure S7). Thereby, the effect of different Pt loadings on the catalytic performance was excluded. The heptane isomerization was performed at various reaction temperatures ranging from 533 to 693 K, following the procedure described elsewhere.[28] The product stream contained various cracking products (C_1−C_6), C_7 branched isomers (*i*-C_7) and the remaining *n*-C_7 reactant. The *i*-C_7 yield (mol %) is plotted as a function of the reaction temperature in Figure 3A. As this result shows, the nanosponge

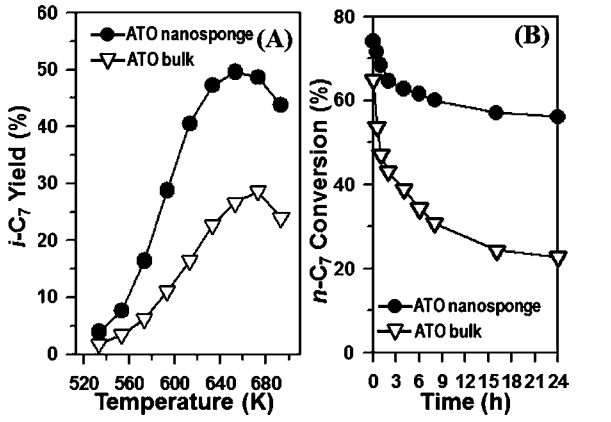

Figure 3. (A) Yield of heptane isomers plotted as a function of reaction temperature in C_7 hydroisomerization over Pt/SAPO catalysts (reaction condition: WHSV = 6.8 h^{-1}, H_2/*n*-C_7 molar ratio = 20, without significant catalytic deactivation detected). (B) *n*-C_7 conversion to *i*-C_7 and cracked products plotted as a function of reaction time (reaction condition: WHSV = 6.8 h^{-1}, H_2/*n*-C_7 molar ratio = 3, 673 K, with catalytic deactivation as shown).

catalyst exhibited a maximum *i*-C_7 yield of 51% at 653 K. The yield decreased above this temperature, due to severe cracking of hydrocarbons. On the other hand, bulk Pt/SAPO exhibited a maximum yield of only 28%. The high yield of *i*-C_7 with nanosponge may be explained by very short diffusion path length for branched products to escape before cracking, as in Pt/MFI zeolite nanosheets.[28] In addition to the high isomer yield, the nanosponge Pt/SAPO catalyst exhibited the advantage of longer catalytic activity, as shown in Figure 3B.

Similar to the aforementioned SAPO synthesis, the addition of $Cr(OAc)_2$ into the synthesis gel composition for the ATO nanosponge resulted in partial substitution of Al with Cr. The CrAPO nanosponge, as synthesized in this manner, exhibited a light-green color indicating the presence of Cr (III) species.[29] A CoAPO sample of the same ATO nanosponge was also synthesized using $Co(OAc)_2$. The CoAPO sample was bluish, indicating incorporation of Co (II). The diffuse reflectance UV−vis spectra of the CrAPO and CoAPO samples displayed the distinct absorption bands, like a fingerprint, indicating the 3d transition-metal elements in frameworks (Figure S8).[29,30] In addition, we were able to synthesize a crystalline GaPO material, using gallium oxide, phosphoric acid, and $8N^4$. The remaining synthesis conditions were exactly the same as those

dx.doi.org/10.1021/ja403580j | J. Am. Chem. Soc. 2013, 135, 8806−8809

used for the ATO nanosponge in Table 1. This GaPO sample (as synthesized) exhibited a wide-angle XRD pattern which was assigned to a zeolite-like crystalline framework structure belonging to the $P6_3/mmc$ space group (a = 1.24 nm, b = 1.68 nm, c = 1.68 nm) (Figure S9). TEM images of the GaPO sample indicated a disordered mesostructure, similar to the ATO nanosponge in Figure 2B (Figure S10). However, the microporous GaPO framework collapsed to a nonporous structure upon calcination at 823 K. The low thermal stability of GaPO framework is due to strong metallic nature of Ga as compared to Al in AlPOs.

In conclusion, the organic multiamine and multiammonium compounds presented in this work can perform the hierarchical structure-directing function for the formation of porous aluminum phosphates and related inorganic phosphates. From the hierarchical structures of the resultant phosphates, it can be inferred that the amine (or ammonium) molecules were assembled into a micelle with a specific morphology. The micellization, as in a surfactant, caused the upper-level (i.e., meso-level) structure-directing function. At the same time, individual amine groups within the micelle performed the lower-level structure-directing function for formation of microporous crystalline AlPOs. Three types of AlPO frameworks (AEL, AFI and ATO) were actually obtained in two types of mesostructured architectures (nanosheets and nanosponges). It is reasonable that the hierarchical structure-directing strategy could be extended to other AlPO frameworks and mesostructures. The thicknesses of the AlPO nanosheets and nanosponge frameworks can be tailored according to the number of the AlPO structure-directing modules in an amine. The synthesis strategy can be further extended to various inorganic phosphate materials with structural hierarchy for enhanced nanoporous functionalities, such as SAPOs, GaPO, and transition-metal-containing AlPOs. Such ultrathin phosphates (2−5 nm as demonstrated with AlPOs) would have various potential applications. A large number of phosphinol groups on the surface would be useful for metal coordination and organic functionalization. Catalytic applications after supporting transition-metal nanoparticles would be considerable, as demonstrated with Pt/SAPO nanosponge.

■ ASSOCIATED CONTENT

Supporting Information

Experimental procedures and results. This material is available free of charge via the Internet at http://pubs.acs.org.

■ AUTHOR INFORMATION

Corresponding Author

rryoo@kaist.ac.kr

Notes

The authors declare no competing financial interest.

■ ACKNOWLEDGMENTS

This work was supported by the Institute for Basic Science in Korea.

■ REFERENCES

(1) Cheetham, A. K.; Férey, G.; Loiseau, T. *Angew. Chem. Int .Ed.* **1999**, *38*, 3268.
(2) Natarajan, S.; Mandal, S. *Angew. Chem., Int. Ed.* **2008**, *47*, 4798.
(3) Pastore, H. O.; Coluccia, S.; Marchese, L. *Annu. Rev. Mater. Res.* **2005**, *35*, 351.
(4) Suchanek, W.; Yoshimura, M. *J. Mater. Res.* **1998**, *13*, 94.
(5) Kalita, S. J.; Bhardwaj, A.; Bhatt, H. A. *Mater. Sci. Eng., C* **2007**, *27*, 441.
(6) Barger, P. T.; Wilson S. T.; Reynolds, T. M. U.S. Patent 5 912 393, 1999.
(7) Mériaudeau, P.; Tuna, V. A.; Nghiem, V. T.; Lai, S. Y.; Hung, L. N.; Naccache, C. *J. Catal.* **1997**, *169*, 55.
(8) Padhi, A. K.; Nanjundaswamy, K. S.; Goodenough, J. B. *J. Electrochem. Soc.* **1997**, *144*, 1188.
(9) Sun, C.; Rajasekhara, S.; Goodenough, J. B.; Zhou, F. *J. Am. Chem. Soc.* **2011**, *133*, 2132.
(10) Zhang, S.; Gonsalves, K. E. *J. Mater. Sci.: Mater. Med.* **1997**, *8*, 25.
(11) Olszta, M. J.; Gheng, X.; Jee, S. S.; Kumar, R.; Kim, Y.-Y.; Kaufman, M. J.; Douglas, E. P.; Gower, L. B. *Mater. Sci. Eng.* **2007**, *58*, 77.
(12) Wilson, S. T.; Lok, B. M.; Messina, C. A.; Cannan, T. R.; Flanigen, E. M. *J. Am. Chem. Soc.* **1982**, *104*, 1146.
(13) Lok, B. M.; Messina, C. A.; Patton, R. L.; Gajek, R. T.; Cannan, T. R.; Flanigen, E. M. *J. Am. Chem. Soc.* **1984**, *106*, 6092.
(14) Yu, J.; Xu, R. *Chem. Soc. Rev.* **2006**, *35*, 593.
(15) Predescu, L.; Tezel, F. H.; Chopra, S. *Adsorption* **1996**, *3*, 7.
(16) Weckhuysen, B. M.; Rao, R. R.; Martens, J. A.; Schoonheydt, R. A. *Eur. J. Inorg. Chem.* **1999**, 565.
(17) Fan, Y.; Xiao, H.; Shi, G.; Liu, H.; Bao, X. *J. Catal.* **2012**, *285*, 251.
(18) Yang, S.-M.; Wu, Y. M. *Appl. Catal., A* **2000**, *192*, 211.
(19) Kim, J.; Bhattacharjee, S.; Jeong, K.-E.; Jeong, S.-Y.; Choi, M.; Ryoo, R.; Ahn, W.-S. *New J. Chem.* **2010**, *34*, 2971.
(20) Pérez-Ramirez, J.; Christensen, C. H.; Egeblad, K.; Christesen, C. H.; Groen, J. C. *Chem. Soc. Rev.* **2008**, *37*, 2530.
(21) Choi, M.; Na, K.; Kim, J.; Sakamoto, Y.; Terasaki, O.; Ryoo, R. *Nature* **2009**, *461*, 246.
(22) Na, K.; Choi, M.; Park, W.; Sakmoto, Y.; Terasaki, O.; Ryoo, R. *J. Am. Chem. Soc.* **2010**, *132*, 4169.
(23) Na, K.; Park, W.; Seo, Y.; Ryoo, R. *Chem. Mater.* **2011**, *23*, 1273.
(24) Jung, J.; Jo, C.; Cho, K.; Ryoo, R. *J. Mater. Chem.* **2012**, *22*, 4637.
(25) Kim, J.; Park, W.; Ryoo, R. *ACS Catal.* **2011**, *1*, 337.
(26) Kamata, H.; Takahashi, K.; Odenbrand, C. U. I. *Catal. Lett.* **1998**, *53*, 65.
(27) Cabeza, A.; Ouyang, X.; Sharma, C. V. K.; Aranda, M. A. G.; Bruque, S.; Clearfield, A. *Inorg. Chem.* **2002**, *41*, 2325.
(28) Kim, J.; Kim, W.; Seo, Y.; Kim, J.-C.; Ryoo, R. *J. Catal.* **2013**, *301*, 187.
(29) Kornatowski, J.; Zadrozna, G.; Rozwadowski, M.; Zibrowius, B.; Marlow, F.; Lercher, J. A. *Chem. Mater.* **2011**, *13*, 4447.
(30) Thomson, S.; Luca, V.; Howe, R. *Phys. Chem. Chem. Phys.* **1999**, *1*, 615.